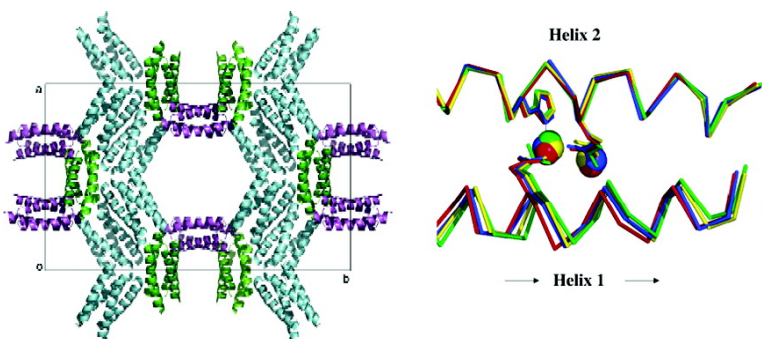Article

Response of a Designed Metalloprotein to Changes in Metal Ion Coordination, Exogenous Ligands, and Active Site Volume Determined by X-ray Crystallography

Silvano Geremia, Luigi Di Costanzo, Lucio Randaccio, Donald E. Engel, Angela Lombardi, Flavia Nastri, and William F. DeGrado

More About This Article

Additional resources and features associated with this article are available within the HTML version:

- Supporting Information
- Links to the 2 articles that cite this article, as of the time of this article download
- Access to high resolution figures
- Links to articles and content related to this article
- Copyright permission to reproduce figures and/or text from this article

View the Full Text HTML

J|A|C|S

A R T I C L E S

Response of a Designed Metalloprotein to Changes in Metal Ion Coordination, Exogenous Ligands, and Active Site Volume Determined by X-ray Crystallography

Silvano Geremia,*,† Luigi Di Costanzo,† Lucio Randaccio,† Donald E. Engel,‡
Angela Lombardi,§ Flavia Nastri,§ and William F. DeGrado*,⊥

*Contribution from the Centre of Excellence in Biocrystallography, Department of Chemical
Science, University of Trieste, Via L. Giorgieri 1, I-34127 Trieste, Italy, Department of Physics
and Astronomy, and Department of Biochemistry and Biophysics, University of Pennsylvania,
Philadelphia Pennsylvania 19104, and Department of Chemistry, University of Napoli
''Federico II'', Complesso Universitario Monte S. Angelo, Via Cynthia 45, I-80126 Napoli, Italy*

Received June 24, 2005; E-mail: geremia@units.it; wdegrado@mail.med.upenn.edu

Abstract: The de novo protein DF1 is a minimal model for diiron and dimanganese metalloproteins, such as soluble methane monooxygenase. DF1 is a homodimeric four-helix bundle whose dinuclear center is formed by two bridging Glu side chains, two chelating Glu side chains, and two monodentate His ligands. Here, we report the di-Mn(II) and di-Co(II) derivatives of variants of this protein. Together with previously solved structures, 23 crystallographically independent four-helix bundle structures of DF1 variants have been determined, which differ in the bound metal ions and size of the active site cavity. For the di-Mn(II) derivatives, as the size of the cavity increases, the number and polarity of exogenous ligands increases. This collection of structures was analyzed to determine the relationship between protein conformation and the geometry of the active site. The primary mode of backbone movement involves a coordinated tilting and sliding of the first helix in the helix−loop−helix motif. Sliding depends on crystal-packing forces, the steric bulk of a critical residue that determines the dimensions of the active site access cavity, and the intermetal distance. Additionally, a torsional motion of the bridging carboxylates modulates the intermetal distance. This analysis provides a critical evaluation of how conformation, flexibility, and active site accessibility affect the geometry and ligand-binding properties of a metal center. The geometric parameters defining the DF structures were compared to natural diiron proteins; DF proteins have a restricted active site cavity, which may have implications for substrate recognition and chemical stability.

Introduction

Metalloproteins help to catalyze some of the most difficult biological reactions. They tune reactivity by using different metal ions with specific redox states, different ligands or geometric arrangements, and a particular protein environment. In the last two decades, there has been an increasing interest in the redesign of existing metal-binding sites in proteins and the introduction of metals into folded proteins/peptides. In particular, de novo design of artificial metalloproteins has contributed significantly to our understanding of fundamental principles of chemistry and biology governing protein folding,[1−14] while simultaneously laying the groundwork for the development of novel catalysts[15−19] and biosensors.[6,20−22]

† University of Trieste.
‡ Department of Physics and Astronomy, University of Pennsylvania.
§ University of Napoli ''Federico II''.
⊥ Department of Biochemistry and Biophysics, University of Pennsylvania.

(1) Lee, K. H.; Matzapetakis, M.; Mitra, S.; Marsh, E. N.; Pecoraro, V. L. *J. Am. Chem. Soc.* **2004**, *126*, 9178−9179.
(2) Pokala, N.; Handel, T. M. *J. Struct. Biol.* **2001**, *134*, 269−281.
(3) Moffet, D. A.; Hecht, M. H. *Chem. Rev.* **2001**, *101*, 3191−3203.
(4) Baltzer, L.; Nilsson, H.; Nilsson, J. *Chem. Rev.* **2001**, *101*, 3153−3163.
(5) Kaplan, J.; DeGrado, W. F. *Proc. Natl. Acad. Sci. U.S.A.* **2004**, *101*, 11566−11570.
(6) DeGrado, W. F.; Summa, C. M.; Pavone, V.; Nastri, F.; Lombardi, A. *Annu. Rev. Biochem.* **1999**, *68*, 779−819.
(7) Baltzer, L.; Nilsson, J. *Curr. Opin. Biotechnol.* **2001**, *12*, 355−360.
(8) Hill, R. B.; Raleigh, D. P.; Lombardi, A.; DeGrado, W. F. *Acc. Chem. Res.* **2000**, *33*, 745−754.
(9) Anderson, L. K.; Caspersson, M.; Baltzer, L. *Chem.−Eur. J.* **2002**, *8*, 3687−3697.
(10) Peluso, S.; Ruckle, T.; Lehmann, C.; Mutter, M.; Peggion, C.; Crisma, M. *ChemBioChem* **2001**, *2*, 432−437.
(11) Kiyokawa, T.; Kanaori, K.; Tajima, K.; Koike, M.; Mizuno, T.; Oku, J. I.; Tanaka, T. *J. Pept. Res.* **2004**, *63*, 347−353.
(12) Ghosh, D.; Pecoraro, V. L. *Inorg. Chem.* **2004**, *43*, 7902−7915.
(13) Ghirlanda, G.; Osyczka, A.; Liu, W. X.; Antolovich, M.; Smith, K. M.; Dutton, P. L.; Wand, A. J.; DeGrado, W. F. *J. Am. Chem. Soc.* **2004**, *126*, 8141−8147.
(14) Carey, J. R.; Ma, S. K.; Pfister, T. D.; Garner, D. K.; Kim, H. K.; Abramite, J. A.; Wang, Z.; Guo, Z.; Lu, Y. *J. Am. Chem. Soc.* **2004**, *126*, 10812−10813.
(15) Johnsson, K.; Allemann, R. K.; Widmer, H.; Benner, S. A. *Nature* **1993**, *365*, 530−532.
(16) Allert, M.; Baltzer, L. *ChemBioChem* **2003**, *4*, 306−318.
(17) Andersson, L. K.; Dolphin, G. T.; Baltzer, L. *ChemBioChem* **2002**, *3*, 741−751.
(18) Bolon, D. N.; Mayo, S. L. *Proc. Natl. Acad. Sci. U.S.A.* **2001**, *98*, 14274−14279.
(19) Benson, D. E.; Wisz, M. S.; Hellinga, H. W. *Proc. Natl. Acad. Sci. U.S.A.* **2000**, *97*, 6292−6297.
(20) Looger, L. L.; Dwyer, M. A.; Smith, J. J.; Hellinga, H. W. *Nature* **2003**, *423*, 185−190.
(21) Benson, D. E.; Wisz, M. S.; Hellinga, H. W. *Curr. Opin. Biotechnol.* **1998**, *9*, 370−376.
(22) Dwyer, M. A.; Looger, L. L.; Hellinga, H. W. *Science* **2004**, *304*, 1967−1971.
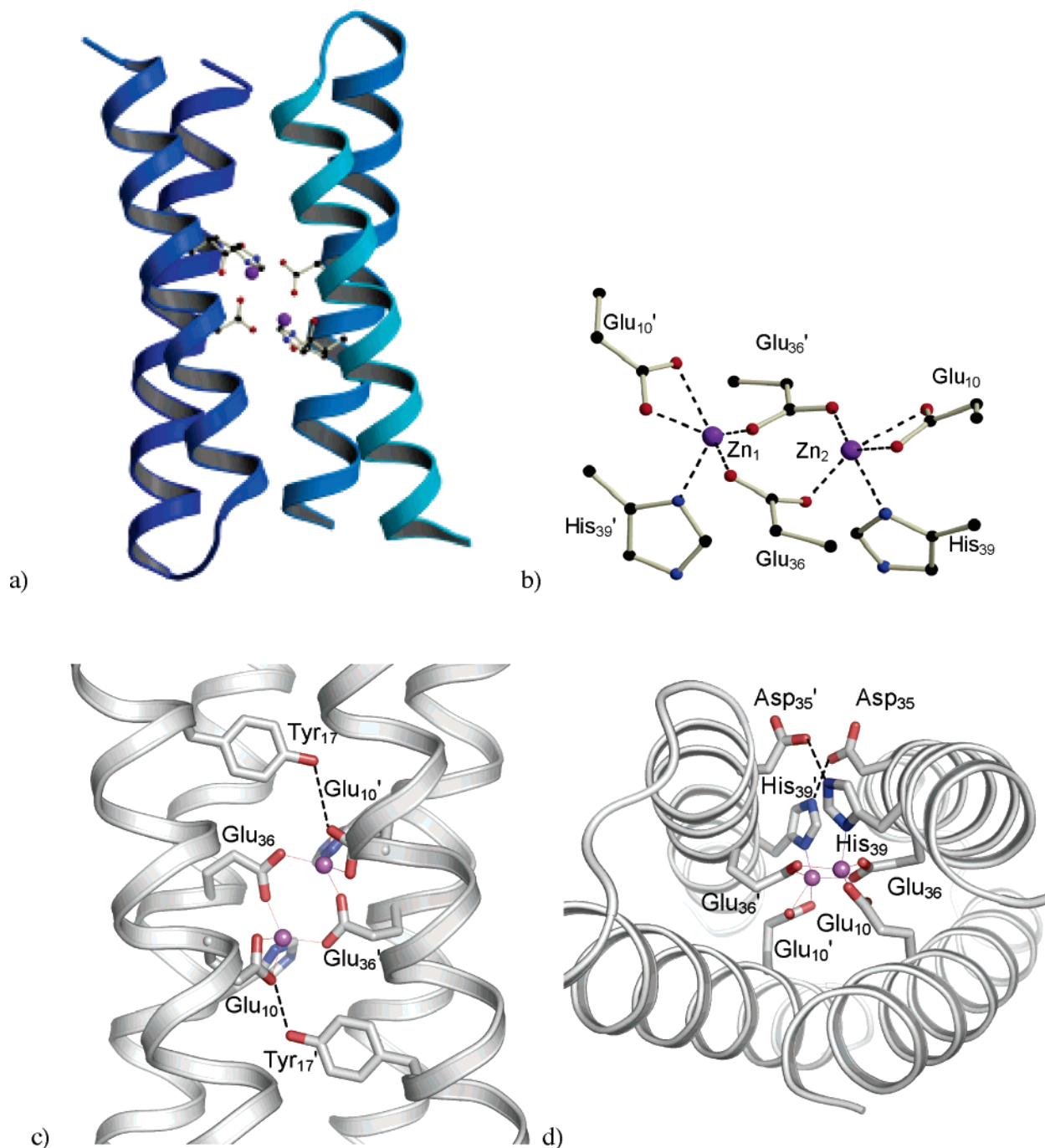
Figure 1. X-ray structure of di-Zn(II)-DF1 (pdb code 1ec5). (a) Representation of the secondary structure with the dimetal center in the core of the four-helix bundle. (b) The coordination environment of the dimetal center. (c, d) Second-shell interaction observed in the X-ray structures of DF1.

Previously, we have focused our studies on a very simple model protein, DF1,[23] which is intended as a model of the primordial precursor from which the functionally diverse class of diiron and dimanganese proteins, such as ferritins, ruberythrin, the R2 subunit of ribonucleotide reductase, and alkane hydroxylases, evolved. This model protein (Figure 1a) idealizes the pseudo 2-fold symmetry observed in the four-helix bundle motif found in several metalloproteins.[24-27] DF1 is a homodimer of

helix−loop−helix hairpins (four-helix bundle) assembled to form a site similar to the binuclear iron site of bacterioferritin,[25] ribonucleotide reductase,[28] and methane monooxygenase[29] (Figure 1b). Each subunit (48 residues) in DF1 contains an E−X−X−H sequence in helix 2, which donates a His side chain ligand and a bridging carboxylate to the site. A second carboxylate from helix 1 provides an additional metal-coordinating ligand. Several metal ions have high affinity to the Glu_4-His_2 site.[23] In particular, divalent ions such as Fe^{2+}, Mn^{2+}, Co^{2+},

(23) Lombardi, A.; Summa, C. M.; Geremia, S.; Randaccio, L.; Pavone, V.; DeGrado, W. F. *Proc. Natl. Acad. Sci. U.S.A.* **2000**, *97*, 6298−6305.
(24) Holmes, M. A.; Stenkamp, R. E. *J. Mol. Biol.* **1991**, *220*, 723−737.
(25) Frolow, F.; Kalb, A. J.; Yariv, J. *Nat. Struct. Mol. Biol.* **1994**, *1*, 453−460.
(26) Holmes, M. A.; Letrong, I.; Turley, S.; Sieker, L. C.; Stenkamp, R. E. *J. Mol. Biol.* **1991**, *218*, 583−593.
(27) Nordlund, P.; Eklund, H. *Curr. Opin. Struct. Biol.* **1995**, *5*, 758−766.
(28) Strand, K. R.; Karlsen, S.; Kolberg, M.; Rohr, A. K.; Gorbitz, C. H.; Andersson, K. K. *J. Biol. Chem.* **2004**, *279*, 46794−46801.
(29) Whittington, D. A.; Lippard, S. J. *J. Am. Chem. Soc.* **2001**, *123*, 827−838.

Ni^{2+}, and Zn^{2+} fit the geometrical environment of this binuclear site well and balance glutamate negative charges.

The assembly of the antiparallel four-stranded coiled coil, which forces the coordinating residues into close proximity in the core of the protein, is stabilized by essential hydrophobic interactions between residues flanking this site, and the protein is folded, even in the absence of metal ions. A number of second-shell ligands also form hydrogen-bonded interactions with the primary ligands, stabilizing their conformations in the core of the protein (Figure 1, parts c and d). A side chain at position 13 in DF1 lines the bottom of the active site cleft and determines the accessibility of the dimetal site. By varying the nature of this residue, it has been possible to introduce phenol oxidase activity into a member of the DF family of proteins;[5] thus, it is important to determine how the nature of this residue affects both the structure of the bundle as well as the nature of the metal-binding site.

Previously we examined the crystal structures of the di-Zn-(II) derivative of DF1 with Leu at position 13 (the wild type)[23] and the di-Mn(II) derivative with Ala and Gly at this position.[30,31] To unambiguously determine how these changes in sequence affect the metal ion coordination, we have now determined the structure of the di-Mn(II) derivative of DF1 with Leu at position 13. We also describe the structure of the di-Co(II) derivative of DF1-L13A. These proteins tend to crystallize in space groups with a large number of independent monomers in the unit cell, allowing comparison of structures with identical sequences as well as closely related derivatives of the same sequence. Thus, this ensemble of structures allows a critical evaluation of how conformation, flexibility, and active site accessibility affect the geometry and ligand-binding properties of a metal center.

Experimental Section

Synthesis and Crystallization. DF1 and the DF1-L13A derivative were chemically synthesized by using the Fmoc protocols as previously described[30] and purified by reversed-phase HPLC. Lyophilized DF1 and DF1-L13A were not completely soluble in water and were dissolved in DMSO to obtain solutions of 100 mg/mL concentration. Both the solutions were diluted 10-fold with water and centrifuged to remove the undissolved materials. Crystals were grown at 277 K by the vapor diffusion hanging drop technique. The drops were prepared by adding 2 μL of the peptide solution (1.5 mM) and 2 μL of reservoir solution containing PEG 400, metal acetate (Mn(CH$_3$COO)$_2$ or Co(CH$_3$COO)$_2$) 30 mM, and Tris−HCl 0.1 M (pH 7.5). The drops were routinely equilibrated against 1.0 mL of reservoir solution. The crystallization conditions were optimized to yield large three-dimensional crystals. In particular, pale pink crystals of di-Mn(II)-DF1 appeared within 8 days and grew to dimensions of 0.3 × 0.3 × 0.1 mm^3 after 3 weeks using PEG 400 32% w/v; whereas rod shaped crystals of di-Co(II)-DF1-L13A grew to dimensions typically of 0.3 × 0.07 × 0.07 mm^3 after 1 month from a reservoir containing PEG 400 43% w/v.

Data Collection and Analysis. X-ray diffraction experiments were carried out at the Elettra synchrotron. The crystals were harvested into mother liquor with a small loop of fine rayon fiber and flash-frozen in a stream of N$_2$ at 100 K. Diffraction data were collected using a monochromatic radiation with wavelength of 1.200 Å and a MAR Research 345 mm imaging plate as detector. The determination of unit

(30) Di Costanzo, L.; Wade, H.; Geremia, S.; Randaccio, L.; Pavone, V.; DeGrado, W. F.; Lombardi, A. *J. Am. Chem. Soc.* **2001**, *123*, 12749−12757.
(31) DeGrado, W. F.; Di Costanzo, L.; Geremia, S.; Lombardi, A.; Pavone, V.; Randaccio, L. *Angew. Chem., Int. Ed.* **2003**, *42*, 417−420.

Table 1. Summary of Space Groups, Unit Cells, Independent Monomers, and V_M in DF1 Structures[a]

structure	space group	a (Å)	b (Å)	c (Å)	independent monomers.	V_M (Å^3/ cm^3)	PDB code	crystal packing
di-Mn(II)-DF1	C222$_1$	88.89	149.18	38.58	4	2.57	1ovr	A
di-Co(II)-DF1-L13A (form 1)	C222$_1$	89.78	147.72	37.60	4	2.66	1ovu	A
di-Mn(II)-DF1-L13G	P2$_1$2$_1$2$_1$	38.20	89.30	146.40	8	2.68	1lt1	A
di-Zn(II)-DF1	C222$_1$	36.07	89.16	79.89	3	1.82	1ec5	B
di-Mn(II)-DF1-L13A (form 2)	C222$_1$	37.12	112.45	79.88	3	2.37	1jmb	B
di-Mn(II)-DF1-L13A (form 1)	P2$_1$2$_1$2$_1$	37.38	80.12	99.93	6	2.13	1jm0	B
di-Co(II)-DF1-L13A (form 2)	P2$_1$2$_1$2$_1$	36.92	80.05	96.62	6	2.03	1ovv	B

[a] These polymorphic structures can be classified with respect to the crystal packing in two groups, the less compact crystal packing A and the more compact crystal packing B (see Figure 2).

Table 2. X-ray Data Collection and Refinement Statistics (Highest Resolution Shell in Parentheses)

	di-Co(II)-DF1-L13A form 1	di-Co(II)-DF1-L13A form 2	di-Mn(II)-DF1
resolution range (Å)	43.2−3.1	33.3−2.9	76.4−3.0
total reflections	17041	37159	12075
unique reflections	4679	6492	5371
completeness (%)	97.7 (97.7)	96.8 (89.0)	98.1 (98.1)
I/σ (I)	5.9 (1.9)	11.2 (3.1)	16.5 (7.0)
multiplicity	3.6 (3.8)	5.7 (5.4)	2.2 (2.2)
R-merge (I) (%)	23.6 (51.5)	10.9 (57.3)	5.1 (16.8)
refinement			
R-factor (%), R-free (%)	24.7, 30.4	26.7, 32.0	22.5, 30.5
ave B factor			
main chain, side chain	57.1, 60.6	60.0, 63.1	30.8, 33.8
RMS deviation			
bond lengths (Å), bond angles (deg)	0.025, 2.88	0.028, 2.52	0.023, 1.86
protein atom	1652	2478	1664
metal ions, water molecules	7, 10	7, 7	5, 38

cell parameters, integration of reflection intensities, and data scaling were performed using MOSFLM and SCALA from the CCP4 program suite.[32] The crystal of di-Mn(II)-DF1 belongs to the orthorhombic space group C222$_1$, with unit cell parameters $a = 89.00$; $b = 149.46$; $c = 38.60$ Å (Table 1).

The analysis of the diffraction pattern of two crystals of di-Co(II)-DF1-L13A obtained in the same crystallizing drop revealed the presence of two different crystal forms (1 and 2).[33] The diffraction pattern of crystal form 1 of di-Co(II)-DF1-L13A was indexed using a face-centered orthorhombic unit cell ($a = 89.83$; $b = 147.98$; $c = 37.60$ Å) with systematic absences in agreement with the C222$_1$ space group. Analysis of the diffraction data of form 2 reveals that the crystal has a primitive orthorhombic Bravais lattice ($a = 36.92$; $b = 80.05$; $c = 96.62$ Å) with systematic absences in agreement with the P2$_1$2$_1$2$_1$ space group (Table 1).

Structure Determination and Refinement. Several attempts to solve the phasing problem of the di-Co(II)-DF1-L13A (form 1 and 2) through molecular replacement, starting from the di-Zn(II)-DF1 model (pdb code = 1ec5), failed due to the relatively low resolution of the data (Table 2) and the combination of crystallographic and noncrystallographic symmetries (Table 1).[33] Nevertheless, the phases of the form 1 structure were assigned using the group and minimal nonisomorphic supergroup relation between the space group of the previously determined di-Mn(II)-DF1-L13G structure (Table 1) and the space group of this form as recently described.[33] Di-Co(II)-DF1-L13A form

(32) Collaborative Computational Project, Number 4. *Acta Crystallogr., Sect. D* **1994**, *50*, 760−763.
(33) Di Costanzo, L.; Forneris, F.; Geremia, S.; Randaccio, L. *Acta Crystallogr., Sect. D* **2003**, *59*, 1435−1439.

1 crystallizes with four crystallographically independent monomers in the asymmetric unit. Form 2 crystallizes with six crystallographically independent monomers in the asymmetric unit (Table 1). Form 2 is isomorphic to form 1 of di-Mn(II)-DF1-L13A (Table 1). The structure was also solved by its group and maximal nonisomorphic subgroup relation with the space group of form 2 of di-Mn(II)-DF1-L13A.[33] The structure of di-Mn(II)-DF1 is isomorphic to that of di-Co(II)-DF1-L13A form 1 (Table 1). The phases were obtained by rigid body refinement, using REFMAC[32] starting from di-Co(II)-DF1-L13A form 1. The crystal structures of di-Co(II)-DF1-L13A and di-Mn(II)-DF1 were further refined with REFMAC,[32] starting from the respective models obtained at the end of the rigid body refinement.[33] A random subset of data (5%) was omitted from all refinement calculations to provide an assessment of the progress of refinement. All data (no σ cutoff) within the resolution ranges were included in the refinement. Tight NCS restraints were applied in the starting refinement steps. The NCS restraints for specific amino acid side chains were released when large differences in conformation between the independent units were detected in the Fourier maps. Due to low-resolution data, the manual rebuilding was difficult. To facilitate the fitting of the electron density maps and improve the progress of refinement, the models were superimposed on di-Mn(II)-DF1-L13A (form 1). Restrained positional and thermal factor refinement with NCS restraints improved the R-factor and R-free values to those reported in Table 2. The dimanganese and dicobalt centers were identified as a pair of peaks of the electron density (6σ) in the $2F_o - F_c$ map. Analogously, a large electron density peak ($>6\sigma$) in the $F_o - F_c$ maps, external to the metal-binding site and near a carboxylate side chain, were identified as metal ions. Due to the low resolution of the data, only a few solvent water molecules were identified from the $F_o - F_c$ map.

Analysis of Helix Orientations in Four-Helix Bundles. For the purposes of generating geometric parameters, each of the four helices was considered to be composed of 11 sequential residues, with the ligating glutamic acid at the center of these 11. Local helix axis points were calculated following the method in HELANAL,[34] and helix axes were defined as the best fit lines along these points. The bundle axis was defined as the average of the four axes, with axes flipped as necessary to match the general direction of helix 1. In some natural proteins, if a helix was severely distorted, it and its diagonal opposite were not used in calculating the bundle's center of mass and central axis. The $z = 0$ plane was defined as the plane perpendicular to the bundle axis and containing the center of mass of the 44 helical backbone residues. This center of mass was used as the origin.

As a reference point, the helix bundles are oriented in a Cartesian coordinate system; the z axis is the bundle's central axis; the x axis connects the origin to the midpoint of where helices 1 and 1′ pass through the $z = 0$ plane; and the y axis is defined by the cross product of z and x. As in previous studies, the orientation of each helix can now be defined by six parameters, without assuming any symmetrical relationship between the individual helices. These parameters include (1) the phase of the α-helix defined by the position of its central glutamic acid's C-α atom; (2) the distance from the origin to each helix's intercept with the $z = 0$ plane; (3) the angle defined by this intercept, the origin, and the x axis; (4) the distance, along each helix in the C−N direction, from the $z = 0$ plane to projection of the glutamic acid's α-carbon onto the helical axis; (5) the point of closest approach between each helix and the superhelical axis; (6) each helix's crossing angle relative to the central axis.

From this complete set of descriptors a number of derived parameters were also examined, which allow a more physically meaningful description of the bundles (e.g., interhelical distances, helical tilt inward toward the bundle core, helical slant sideways along the bundle's surface).

(34) Bansal, M.; Kumar, S.; Velavan, R. *J. Biomol. Struct. Dyn.* **2000**, *17*, 811−819.
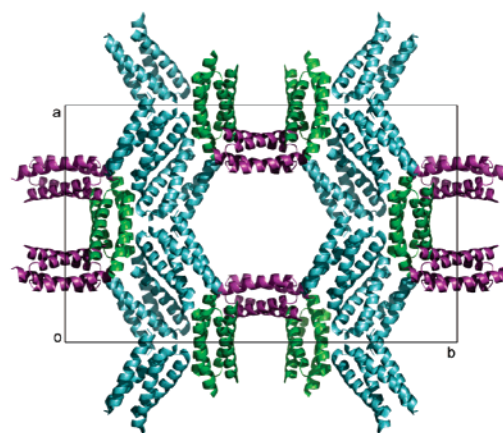
a)
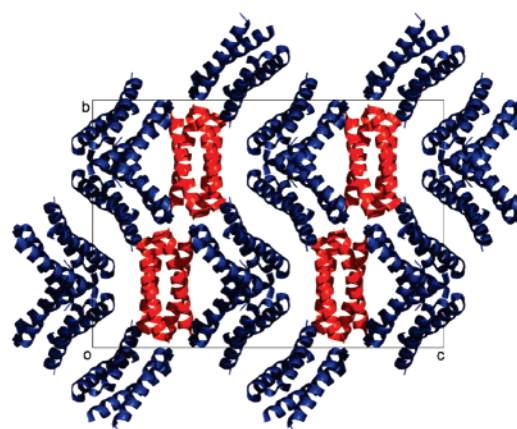
b)

Figure 2. Two different crystal packings observed in DF1 structures: (a) crystal packing of type A found in di-Co(II)-DF1-L13A (form 1) and (b) crystal packing of type B found in di-Mn(II)-DF1-L13A (form 2).

Group/Subgroup Relations and Crystal Packing. In addition to the phasing process, the recognition of group−subgroup relations between space groups of different crystal structures can provide insight into protein packing. With the use of these group−subgroup relations, the four previously reported crystal structures of DF1 derivatives[23,30,31] and the three crystal structures reported in this paper (Table 1) can be classified into two distinct crystal-packing groups: a less compact crystal packing of type A (Figure 2a), and a more compact crystal packing of type B (Figure 2b).

The crystal-packing analysis of these systems is particularly important with respect to the different behavior previously observed for crystallographically independent four-helix bundles and associated with a sliding helix mechanism.[31] The di-Mn(II)-DF1 structure, representative of the less compact (type A) packing, is characterized by peptides having a helix−turn−helix motif assembled in noncovalent homodimers with C_2 symmetry. Figure 2a illustrates a segment of the crystallographic lattice of this protein. The asymmetric unit is composed of four crystallographically independent helical hairpin monomers; two of them form dimeric four-helix bundles with exact crystallographic symmetry (chains A and B, depicted in Figure 2a in green and violet, respectively) while the other two form a pseudosymmetric dimer within the asymmetric unit itself (chains C and D, represented in cyan color in Figure 2a). A similar packing has been observed for the nonisomorphic di-Mn(II)-DF1-L13G crystal structure. This structure has lower crystal symmetry (the $P2_12_12_1$ space group is a maximal nonisomorphic subgroup of the $C222_1$ space group), and as a consequence, the number of crystallographically independent monomers doubles from four to eight. In this case, the asymmetric unit is formed by four pseudosymmetric dimers (note each dimer is a four-helix bundle).
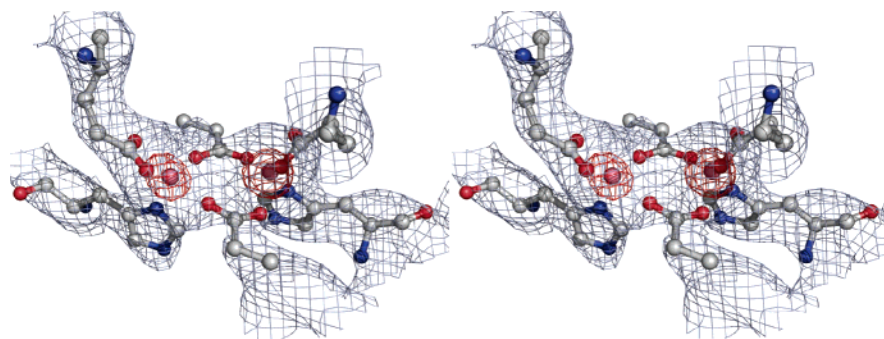
Figure 3. Stereoview of the $2F_o - F_c$ electron density map (contoured at 1.5σ in blue and at 6σ in red) around the dimetal center of di-Co(II)-DF1-L13A (form 2).

We also observed group—subgroup relationships between different DF1 variants that crystallize in the more dense B type packing (Table 1). The form 2 crystals of di-Mn(II)-DF1-L13A provide an example of the B type packing, in this case with a $C222_1$ space group. Figure 2b illustrates a portion of this lattice. The asymmetric unit is composed of three crystallographically independent helical hairpin monomers. One forms dimers with precise symmetry along a 2-fold crystallographic axis (chain A, in red in Figure 2b), while the other two are assembled in pseudosymmetric dimers (chains B and C, in blue in Figure 2b). Similar packing has been observed for the nonisomorphic crystal structure of the analogous cobalt derivative, which crystallizes in $P2_12_12_1$. The lower crystal symmetry found in form 2 of di-Co(II)-DF1-L13A doubles the number of crystallographically independent monomers from three to six. In this case, the asymmetric unit is formed by six helix—loop—helix peptides that assemble to form three pseudosymmetric dimers. Among the type B crystals the *a* edge is relatively constant at approximately 36—37 Å, and the *b* or *c* edge is also constant at approximately 80 Å, but the remaining edge is more variable.

It is apparent from Figure 2 that type B crystal packing is more compact than type A. The Matthews volume (V_M) calculated within these groups agrees, with a higher solvent content in crystals of type A (range 2.57—2.68 Å³/cm³) than in those of type B (1.82—2.37 Å³/cm³). Furthermore, large solvent channels are observed along the shortest crystallographic axes only in crystal packings of type A. This difference has important implications on the structural differences observed between the crystallographically independent units (see below).

As in previous studies, metal ions from the crystallization buffer stabilize many of the interfaces between the individual four-helix bundles. Although the dimetal—DF1 complexes are able to crystallize from solutions containing stoichiometric concentrations of divalent ions (see form 2 of di-Mn(II)-DF1-L13A), an excess of the cation in the crystallization solution improves the crystal diffraction quality (see form 1 of di-Mn(II)-DF1-L13A).[30] Three crystallographically independent "external" cobalt atoms were recognized in the asymmetric unit of di-Co(II)-DF1-L13A form 1, but only one "external" metal ion was recognized in both di-Mn(II)-DF1 and di-Co(II)-DF1-L13A form 2 crystal structures. The coordination geometry observed for these "external" ions is quite variable, and it is highly incomplete in the structures determined at low resolution (Figure S1 of the Supporting Information).

Coordinates have been deposited in the RCSB Data Bank, access numbers: 1ovr for di-Mn(II)-DF1, 1ovu (for form 1) and 1ovv (for form 2) of di-Co(II)-DF1-L13A.

Results and Discussion

Tertiary Structure of Di-Mn(II)-DF1 and Di-Co(II)-DF1-L13A. The three-dimensional molecular structures of di-Mn-(II)-DF1 and di-Co(II)-DF1-L13A are very similar to the previously determined X-ray structures[23,30,31] and to the de novo designed model.[23] This four-helix bundle protein is comprised

of two noncovalently associated helix—loop—helix motifs. The H-bond network of the main chain is consistent with six turns of an α-helix for each element of secondary structure. The superposition of the crystallographically independent monomers shows a very good overlap of the overall structure. The largest differences in the protein structure are ascribable to the conformation of the turn interconnecting the two helices (see above). DF1 was designed with a two-residue interhelical linker (Lys25—Leu26), with an $\alpha_L-\beta$ conformation.[23] However, the turn conformation appears to be more influenced by the crystal environment, and the most recurring conformation found in the DF1 structures is a $\beta-\beta$ conformation of the Val24 and Lys25 residues. Recently, the loop sequences in two additional DF1 derivatives, DF2 and DF2t1, were designed and shown to adopt the desired turn conformations, and details of the analysis and design of these α-helical hairpins are reported by Lahr et al.[35]

The dimetal center in both di-Mn(II)-DF1 and di-Co(II)-DF1-L13A (form 1 and 2) structures appears as the highest pair of peaks in the electron density $2F_o - F_c$ maps (Figure 3).

The electron density of the metal-coordinating groups is well defined in this region of the map and allows the unambiguous positioning of the side chains (Figure 3). The refined Debye—Waller factors of both dimanganese and dicobalt centers, with values similar to those of the coordinating residues, suggest the full occupancy of these sites.

Di-Mn(II) Center. The di-Mn(II) center in di-Mn(II)-DF1 is similar to that found in previous mutant structures,[30,31] but no bridging solvent molecules were observed at the present resolution. Figure 4 compares the environment and geometry of di-Mn(II)-DF1 with the corresponding L13A and L13G variants. Each metal ion is five-coordinate. Glu-36 and 36′ (the apostrophe indicates residues of the second chain) interact with both metal ions in a μ-(1—3) syn—syn bidentate bridging interaction, whereas Glu-10 and 10′ interact in an η_2 chelating manner. His 39 and 39′ complete the liganding environment of each metal ion through the coordination of the N_δ atom. The small variation in metal—ligand distances between this and previously solved di-Mn(II) variants of DF1 is not significant at the current resolution of these X-ray structures.

The electron-dense metal sites are very well localized in the density maps, and the differences in the metal—metal distance can be discussed with more confidence than the metal—ligand distances (Scheme 1).

The long Mn—Mn distances (4.1—4.3 Å) in di-Mn(II)-DF1 are consistent with the lack of a bridging ligand. In the di-Mn-

(35) Lahr, S. J.; Engel, D. E.; Stayrook, S. E.; Maglio, O.; North, B.; Geremia, S.; Lombardi, A.; DeGrado, W. F. *J. Mol. Biol.* **2005**, *346*, 1441—1454.
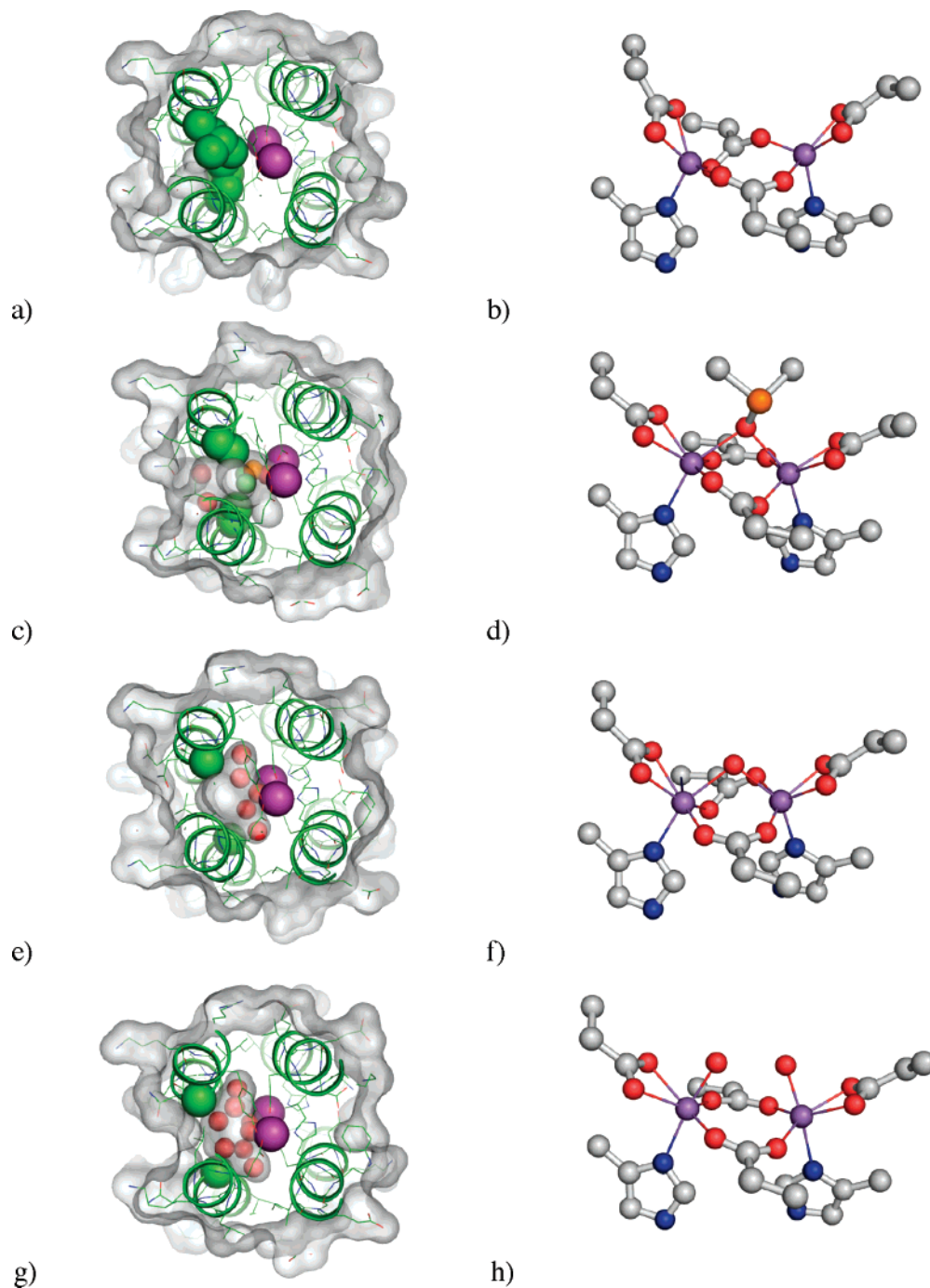
Figure 4. Top view of the active site cavity in DF1 (left side), highlighting the different residues in position 13 (green spheres), key residues to permit the substrate access to the metal ions (violet spheres), and relative coordination geometry of the dimetal center (right side). (a, b) Di-Mn(II)-DF1 with L13 and L13′ which block the substrate channel. (c, d) Di-Mn(II)-DF1-L13A with the access channel that results from the L13A mutation and with a bridging DMSO molecule. (e, f) AB subunit of di-Mn(II)-DF1-L13G with a very large access channel and with a bridging water molecule. (g, h) GH subunit of di-Mn(II)-DF1-L13G with two apically coordinated water molecules.

Scheme 1. Metal–Metal Distances Found in DF1 Structures

Zn---Zn = 3.9 Å   Co---Co = 4.1 Å   Mn---Mn = 4.3 Å

H$_2$O   DMSO   H$_2$O H$_2$O

Mn---Mn = 3.6 Å   Mn---Mn = 3.8 Å   Mn---Mn = 4.2 Å
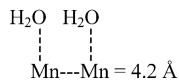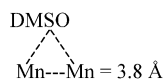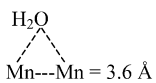
(II)-L13A and L13G variants, the bridging ligands, DMSO and H$_2$O, reduce the Mn–Mn to shorter values (Scheme 1). Furthermore, modeling a hypothetical bridging water molecule in the present structure of di-Mn(II)-DF1 led to a large clash

(2.6 Å) with Leu13. This clash was even more significant when DMSO was introduced as a bridging ligand, or when two waters were modeled as terminal ligands as in di-Mn(II)-DF1-L13G. Thus, the presence of a bulky Leu residue at position 13 of DF1 has prevented the binding of a bridging ligand.

A binuclear manganese site has been found in arginase[36] and manganese catalase[37] enzymes. The Mn cofactor in the catalase is located in a four-helix bundle, whereas the Mn ions in arginase are found at the bottom of a cleft formed with α helices and β sheets. Nevertheless, the catalytic centers are very similar
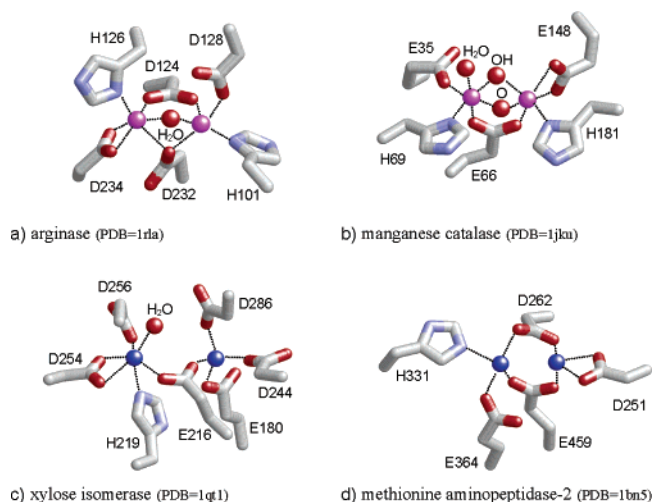
Figure 5. Coordination geometry of the dimetal center observed in natural proteins: (a) di-Mn(II) center in arginase; (b) di-Mn(III) center in manganese catalase; (c) di-Co(II) center in xylose isomerase; (d) di-Co(II) center in methionine aminopeptidase-2.

(Figure 4, parts b, d, f, and h). Several crystal structures are now available for these proteins, also at atomic resolution.[37,38] However, the presence of disorder in the catalytic site and the possibility of radiation damage, leading to a mixture of Mn oxidation states in several of these structures, might conceivably render precise comparisons difficult.[39] Fortunately, both EPR and EXAFS data provide supplementary information to verify the consistency of X-ray structures.[39] In selected di-Mn(II) proteins, the Mn–Mn distances are found in the range of 3.3–3.6 Å, depending on the number and the nature of bridging anions.[36,37,40–43] Shorter distances have been observed for di-Mn(III) forms of dimanganese catalase where bridged oxo and hydroxyl ions are present (3.0–3.4 Å) (Figure 5b).[38,44,45] Cobalt ions play a number of crucial roles in many biological

The B12 proteins, in which the ion is inserted in the corrin ring, are the most-studied cobalt proteins. However, several other proteins containing cobalt in a different form (methionine aminopeptidase, prolidase, nitrile hydratase, glucose isomerase, methylmalonyl-CoA carboxytransferase, aldehyde decarbonylase, lysine-2,3-aminomutase, and bromoperoxidase) have been isolated and characterized.[46] To date, the dicobalt center has been structurally characterized in two "natural" proteins, the bacterial xylose isomerase[47] and the human methionine ami-

nopeptidase-2.[48] Both structures show a highly asymmetric dimetal center (Figure 5, parts c and d). In bacterial xylose isomerase,[47] the Co–Co distance (4.9 Å) is much larger than that found in the human methionine aminopeptidase-2 (3.1 Å).[48] Recently, a short metal–metal distance (3.4 Å) has been reported for the X-ray structure of the mouse R2 ribonucleotide reductase containing two cobalt(II) ions instead of the "natural" diiron center, and EPR data show that this dicobalt site is ferromagnetically coupled.[49] An even closer approach (3.0–3.1 Å) is observed in di-Co(II) methane monooxygenase.[50]

In di-Co(II)-DF1-L13A, one dimer of the six independent units shows a short Co–Co distance (3.6 Å), while the others range from 4.1 to 4.3 Å. The coordination geometry is very similar to that of di-Zn(II)-DF1 and di-Mn(II)-DF1, with two chelating Glu ligands, two 1,3 bridging ligands, and two His ligands, giving a five-coordinate geometry for each metal ion. This coordination is consistent with the visible spectrum of di-Co(II) derivatives of DF1 and DF2, all of which are all consistent with a pentacoordinate geometry.

Correlations between Helix Movements and Metal-Binding Site Geometry. In this and previous papers, we have solved a total of 20 crystallographically independent molecular structures of DF1, DF1-L13A, and DF1-L13G, as well as three structures of the closely related proteins DF2 and DF2t.[35] The metal ions in these proteins included Mn(II), Co(II), Cd(II), and Zn(II). This ensemble of structures, determined in a number of crystal-packing environments, allows systematic investigation of structural variability and how the protein matrix responds to mutations and differences in the metal ion cofactor.

Scheme 1 reports the mean values of the metal–metal distances observed in the X-ray structures of DF1 metalloproteins. In the absence of exogenous ligands, these distances increase (Mn > Co > Zn) with decreasing atomic number. This is consistent with the atomic orbital contraction related to the nuclear charge that permits a closer approach of the bridging protein ligands to the metal ions. Also, additional bridging exogenous ligands can significantly shorten the metal–metal distances (Scheme 1).

How does the protein vary its geometry in response to these differences in metal–metal distances, the presence of exogenous ligands, and the bulk of the side chains lining the active site access channel? To address this question, we examined all structures for the orientation of each helix relative to the central axis of the bundle. We restricted the analysis to an 11-residue segment centered on the active site Glu residue, to identify geometric variations most closely coupled to the metallo site and to minimize variations that are associated with peripheral loops and the ends of the helices.

Previously, we noticed that helix 1 shows more structural variability in the individual crystallographically distinct dimers within the unit cell of di-Mn(II)-DF1-L13G. An analysis of all the DF1 and DF2 structures shows that this helix is able to slide vertically by up to 1.3 Å along a coordinate vertical to the bundle's axis and that this motion alone accounts for approximately 50% of the variation in the coordinates of the

(36) Kanyo, Z. F.; Scolnick, L. R.; Ash, D. E.; Christianson, D. W. *Nature* **1996**, *383*, 554–557.
(37) Barynin, V. V.; Hempsted, P. D.; Vagin, A. A.; Antonyuk, S. V.; Melik-Adamyan, W. R.; Lamzin, V. S.; Harrison, P. M.; Artymiuk, P. J. *J. Inorg. Biochem.* **1997**, *67*, 196.
(38) Barynin, V. V.; Whittaker, M. M.; Antonyuk, S. V.; Lamzin, V. S.; Harrison, P. M.; Artymiuk, P. J.; Whittaker, J. W. *Structure* **2001**, *9*, 725–738.
(39) Wu, A. J.; Penner-Hahn, J. E.; Pecoraro, V. L. *Chem. Rev.* **2004**, *104*, 903–938.
(40) Bewley, M. C.; Jeffrey, P. D.; Patchett, M. L.; Kanyo, Z. F.; Baker, E. N. *Struct. Fold. Des.* **1999**, *7*, 435–448.
(41) Law, N. A.; Caudle, M. T.; Pecoraro, V. L. In *Advances in Inorganic Chemistry*; Sykes, A. G., Ed.; Academic Press: New York, 1999; Vol. 46, pp 305–440.
(42) Khangulov, S. V.; Pessiki, P. J.; Barynin, V. V.; Ash, D. E.; Dismukes, G. C. *Biochemistry* **1995**, *34*, 2015–2025.
(43) Cox, J. D.; Kim, N. N.; Traish, A. M.; Christianson, D. W. *Nat. Struct. Mol. Biol.* **1999**, *6*, 1043–1047.
(44) Whittaker, M. M.; Barynin, V. V.; Igarashi, T.; Whittaker, J. W. *Eur. J. Biochem.* **2003**, *270*, 1102–1116.
(45) Vainshtein, B. K.; Melik-Adamyan, W. R.; Barynin, V. V.; Vagin, A. A.; Grebenko, A. I. *Nature* **1981**, *293*, 411–412.
(46) Kobayashi, M.; Shimizu, S. *Eur. J. Biochem.* **1999**, *261*, 1–9.
(47) Zhu, X.; Teng, M.; Niu, L.; Xu, C.; Wang, Y. *Acta Crystallogr., Sect. D* **2000**, *56* (Part 2), 129–136.

(48) Liu, S.; Widom, J.; Kemp, C. W.; Crews, C. M.; Clardy, J. *Science* **1998**, *282*, 1324–1327.
(49) Strand, K. R.; Karlsen, S.; Andersson, K. K. *J. Biol. Chem.* **2002**, *277*, 34229–34238.
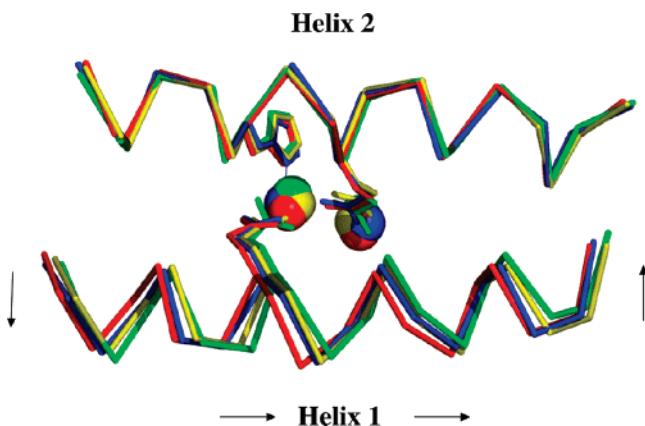(50) Sazinsky, M. H.; Merkx, M.; Cadieux, E.; Tang, S.; Lippard, S. J. *Biochemistry* **2004**, *43*, 16263–16276.

Helix 2

Figure 6. Representative examples of structures of the aligned helix 1/heix 2 interfaces. Helix 2 is relatively immobile, while helix 1 shows more conformational mobility. Two motions account for most of the variation in the coordinates. One movement involves a sliding of helix 1 from left to right as one progresses from the red structure to the green. Concomitantly the helix undergoes a rocking motion, with the green structure moving up on the right and down on the left. The subunits shown are from 1ec5 subunit A (green), 1lt1 subunit H (red), 1lt1 subunit A (yellow), and 1ovr subunit B (blue).
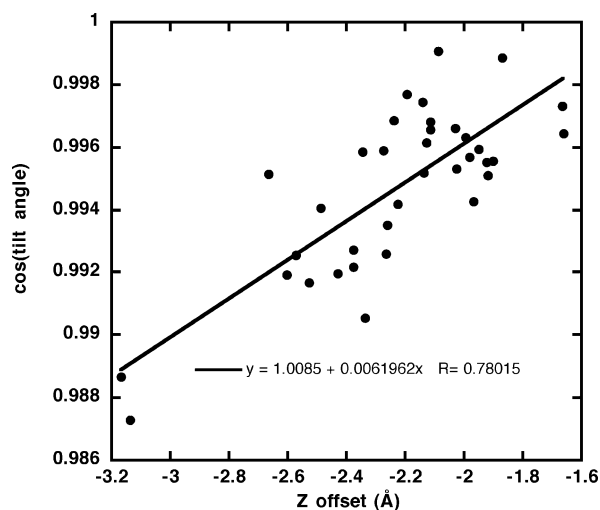

Figure 7. Correlation between translation and tilting motions of helices.

individual protein structures (Figure 6). Analysis of other principle modes identified only one additional movement that contributed significantly to structural variability—a tilt of the C-terminal end of helix 1 toward, and the N-terminal end away from, the bundle axis. The translation and tilting motions are highly correlated (Figure 7; $R = 0.78$), indicating that they are coupled motions.

While these are the two largest movements within the aligned helical bundles, we examined whether other movements might correlate with more specific features of the proteins, such as the intermetal distance and the bulk of the residues lining the substrate access cavity. While the displacement of helix 1 along the long axis of the bundle had previously been shown to correlate with intermetal distance in the DF1-L13G variants, the correlation was much weaker when the entire set of DF1 and DF2 variants was examined ($R = 0.41$). A stronger correlation was observed between the intermetal distance and the dihedral angle between the plane of the bridging Glu carboxylates and the two metal ions (Figure 8). Although the correlation for all crystal structures was modest ($R = 0.59$), all
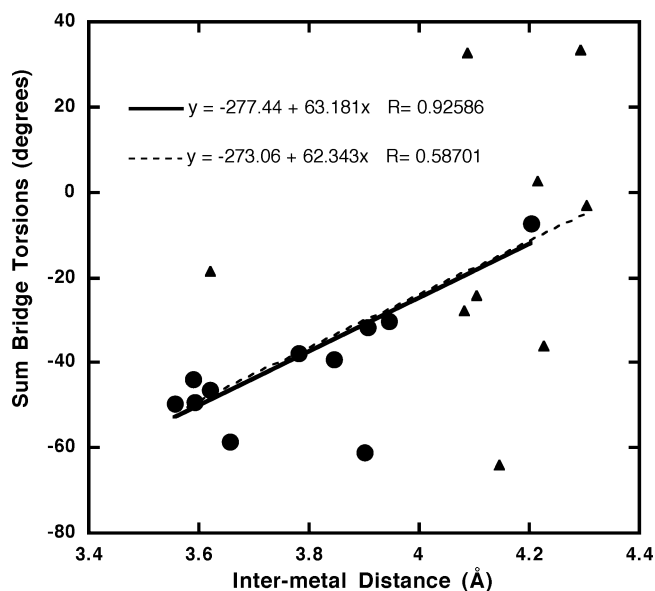

Figure 8. Correlation between the intermetal distances and the sum of the carboxylate plane−dimetal center torsion angle for the two carboxylates. The high-resolution structures are indicated by circles and the lower resolution structures by triangles. The angle is defined by a metal atom, the bimetals' center of mass, the glutamic acid's δ-carbon, and one of the glutamic acid's ϵ-oxygens. The dashed line is the regression line calculated with all data (circles and triangles), and the solid line is calculated for all but the single outlier of the high-resolution structures (triangles). If this outlier is included the correlation coefficient for all high-resolution structures decreases to 0.73.

but one of the outliers are associated with crystal structures with relatively low resolution (>2.5 Å). If these are excluded from the analysis, the slope and intercept do not change appreciably, but the correlation coefficient improves markedly (Figure 8). Thus, by changing the torsional angles of the two Glu carboxylates it is possible to systematically vary the intermetal distance.

The residues at positions 13 and 13′, which define the size of the active site access channel, pack along the helix 1/helix 1′ interface. As the steric bulk of residue 13 is decreased from Leu to Ala, the helix 1−1′ interhelical distance changes only very slightly from a mean of 10.8 ± 0.1 Å (standard error) to 11.0 ± 0.1 Å, respectively. No further change is observed in the variants with Gly at position 13, which have a mean distance of 11.0 ± 0.1 Å. Overall, the degree of coordinate variability between nonequivalent dimers within a single unit cell is comparable to the variability when all of the position 13 variants are examined. Thus, we conclude that the backbone does not move appreciably in response to these mutations. This near complete invariance of the interhelical distances over this series demonstrates the robustness of the DF framework for examining how the solvent accessibility affects the reactivity of the metal ion center.

Influence of Crystal Packing on the Structure of DF1. Previously, we observed a displacement of helices 1 and 1′ in different dimers of the asymmetric unit of di-Mn(II)-DF1-L13G. A shift of the helices was observed in only one of the crystallographically independent units, corresponding to the violet dimer of Figure 2a. Helices 1 and 1′ slide in opposite directions by approximately 0.9 Å along the z axis (the central axis of the bundle), giving rise to a larger distance between the Glu ligands. Coincident with this shifting, the metal ion distances lengthened from approximately 3.6−4.2 Å. The "violet" dimer

Table 3

dimer	mean d_z (Å)	designation	exogenous ligands	mean intermetal distance (Å)
di-Mn(II)-DF1-L13G subunits AB, CD, EF	2.19 (0.09)	relaxed	bridging water	3.59 (0.02)[a]
di-Mn(II)-DF1-L13G subunits GH	3.15 (0.02)	stressed	2 terminal waters	4.20
di-Mn(II)-DF1-L13A subunits AA, CD	2.14 (0.16)	relaxed	none	4.22 (0.01)
Mn(II) DF1-L13A subunit BB	2.57	stressed	none	4.30
di-Co(II)-DF1-L13A form 1 subunits AA, CD	2.33 (0.07)	relaxed	none	4.12(0.02)
di-Co(II)-DF1-L13A form 1 subunit BB	2.66	stressed	none	4.29

[a] When more than one distance is available, a value in parentheses reflects the standard error.

binds two water molecules that are coordinated to the manganese ions trans to the His ligands (Scheme 1; Figure 4h). By contrast, the other dimers bound manganese ions with a bridging solvent molecule (Scheme 1; Figure 4f). We therefore examined the other structures having the crystal packing of A type: di-Mn-(II)-DF1 and di-Co(II)-DF1-L13A form 1. The corresponding "violet" dimer of the di-Mn(II)-DF1 and di-Co(II)-DF1-L13A form 1 structures also has a shift with respect to all other four-helix bundles, but of reduced magnitude, approximately 0.3–0.4 Å. Concomitantly, the metal–metal distances change by 0.1–0.2 Å.

These findings demonstrate the effect of helix-packing forces on the structure of DF1 as well as the metal ligation geometry. The "violet" subunits experience a crystal-packing force that tends to displace helices 1 and 1′ along the z axis away from the origin of the bundle; we refer to this dimer as stressed and the other dimers in the asymmetric unit as relaxed. Table 3 illustrates the intermetal distances and the degree of sliding of helices 1 and 1′ along the z axis (a d_Z value of 0 would place the helix axis projection of the Glu C-α in the x–y plane of the coordinate system) for each of these proteins.

In all the relaxed dimers, the value of d_Z is approximately the same (2.2 ± 0.1 Å), indicating that this helical displacement can accommodate both a close intermetal distance of 3.6 Å observed in the water-bridged di-Mn(II)-DF1-L13G structure as well as the longer distance of 4.2–4.3 Å observed in the di-Co(II)-DF1-L13A form 1 and di-Mn(II)-DF1 structures. In the stressed dimer the value of d_Z increases to 3.15 Å in the di-Mn(II)-DF1-L13G structure, but this value is attenuated to 2.6–2.7 Å in the other structures with side chains larger than Gly at position 13. Examination of the protein structures suggests that the sterics associated with this residue prevent further extension when the residue at position 13 is larger than Gly.

These findings clearly show how solvent accessibility, together with the fold of the protein, determine the structure of the di-Mn(II) cluster. With a large Leu side chain at position 13, exogenous ligands are effectively excluded and each metal ion retains an open chelation site. With Gly at position 13, a large cavity is formed that can accommodate additional exogenous water ligands. In the relaxed conformation, the value of d_Z is sufficient to allow either the close intermetal distance required for a water-bridged cluster or the longer distance (4.2 Å) required for a structure with two terminal water molecules (an equivalent value of d_Z is found in the relaxed forms of di-
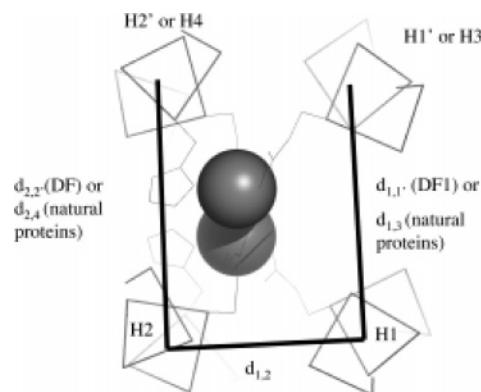
Figure 9. Correspondences between helices in DF and natural four-helix bundle diiron proteins.

Mn(II)-DF1-L13, which has an intermetal distance of 4.2 Å). Evidently, the water-bridged structure is thermodynamically favored in the relaxed L13G variant because of the intrinsic preferences of the metal ion. Only in the stressed L13G variant are the helices sufficiently displaced to exclude the water-bridged di-Mn cluster, causing the metal center to adopt the terminally coordinated structure with a longer intermetal distance.

Comparison of the Structure of DF Proteins to Natural Diiron Proteins. Our geometric parametrization of the diiron four-helix bundle structure allows a facile comparison between the DF and the natural diiron proteins. The orientation of each of the helices comprising their active sites requires six parameters (three rotations and three translations), to uniquely describe the bundle (as described in the Experimental Section). These parameters were examined for both the DF and the natural proteins, to identify areas of high similarity as well as differences between the structures, which were then used to identify physically meaningful changes in terms of helix-packing interactions between the individual helices.

Figures 9 and 10 define and report parameters that show the greatest differences between the natural and the designed proteins. A few parameters that show less marked deviation are also included for comparison. The displacement of the active site C-α of Glu in the direction of the long axis of the bundle is one of the variable parameters in the DF proteins, although it is not as variable as in the natural proteins. Both parameters show peaks at the same positions. The direction of each helical axis relative to the bundle axis was measured in terms of two terms, both evaluated at the x–y plane: one measures the tilt inward toward the main axis of the bundle, and the other measures slant sideways along the bundle surface in a direction orthoganol to the helical axes. Again, the spread of values for the natural proteins was greater than the DF proteins, but both peaked at the same positions.

By contrast, the interhelical distances of the DF proteins, relative to the natural proteins, show several differences, which may be functionally significant. The interface between helix 1 and 1′ of DF proteins forms most of the substrate-binding cavity. Although there is some overlap in the distributions, the interhelical distances of the corresponding helices of natural proteins tend to be larger. A similar trend is seen for the helix 2/helix 2′ interface, where the natural proteins tend to have larger distances than the DF proteins. The converse holds for the helix
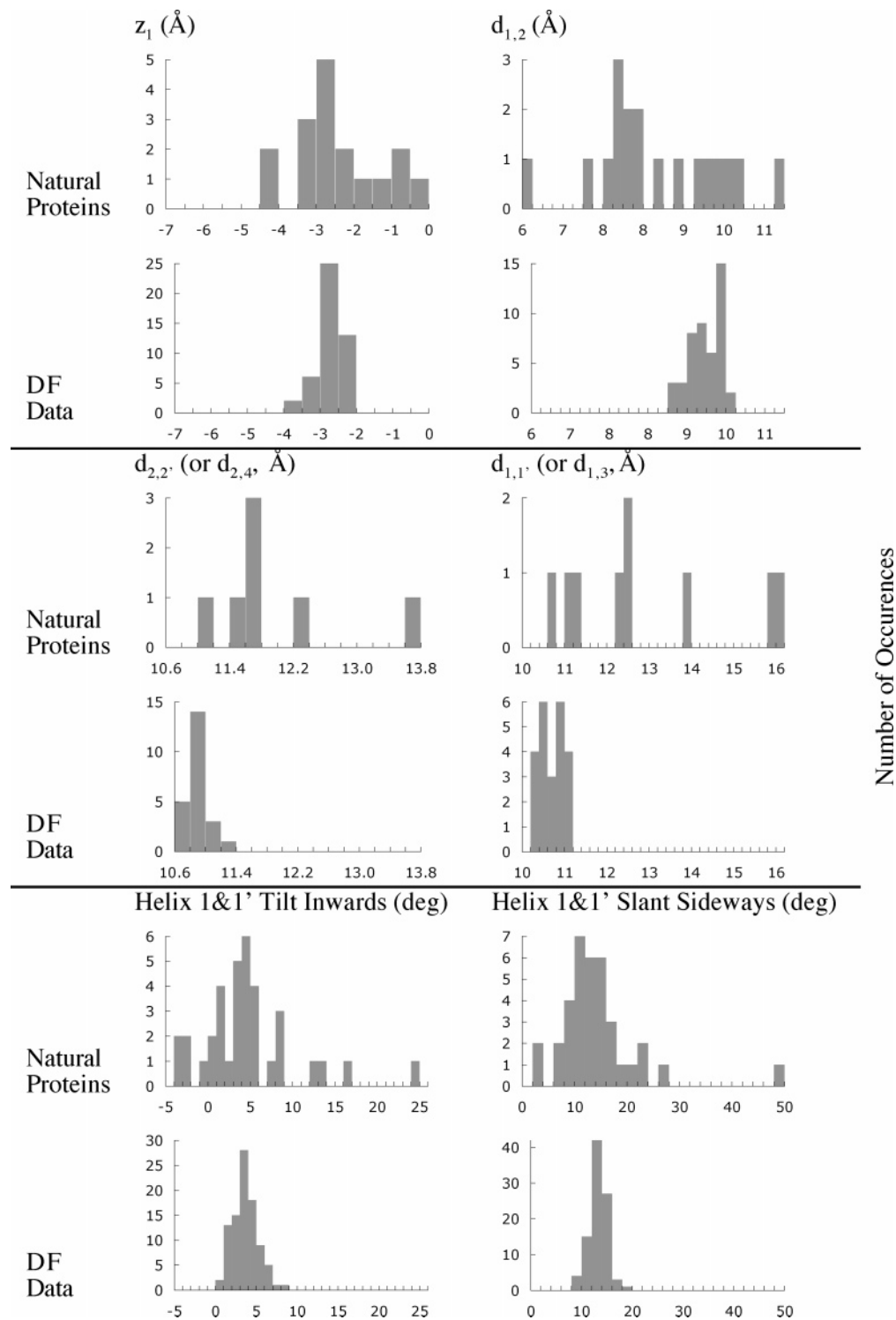
Figure 10. Comparison between DF and natural proteins. The displacement of the active site C-α of Glu in the direction of the long axis of the bundle and the tilt of the helices are the variable parameters in the DF proteins, although it is not as variable as in the natural proteins.

1/helix 2 interface, which tends to be more closely packed in an AlaCoil interaction.[51]

Conclusions

The availability of multiple crystal structures of DF1 and DF2 has allowed an unprecedented examination of how a designed protein can accommodate different metal ions and exogenous

(51) Gernert, K. M.; Surles, M. C.; Labean, T. H.; Richardson, J. S.; Richardson, D. C. *Protein Sci.* **1995**, *4*, 2252−2260.

ligands in its binding site. The overall picture is of a protypical binding site with two bridging carboxylates, two chelating carboxylates, and two monovalent His ligands. An open coordination site on both metal ions provides an attractive site for an approaching dioxygen molecule. Although this is a protypical picture, one observes significant flexibility and more or less deviation from structure to structure, as, for example, the chelating glutamates can distort toward bond distances expected for monovalent ligands. This rather symmetric pro-

typical coordination geometry is also seen in natural diiron proteins (such as ribonucleotide reductase, bacterioferritin, and a desaturase) in cases in which their structures are solved with divalent metal ions bound to their active sites. Again, individual structures will show small variations arising from carboxylate shifts, which in this case may be functional. In the designed structures, we observed the angle between the planes of the bridging Glu ligands as a critical parameter helping to define the metal−metal distance.

This analysis showed the plasticity of the fundamental DF framework, its modes of motion, and the degree of similarity of structure to natural diiron proteins. The structures show significant helix tilting and sliding motions, which may ultimately be important for changes in response to redox shifts and organic substrates. Recently, Sazinsky et al. reported rather large-scale motions in an active site helix in response to different product complexes in the crystal structure of MMO.[50] In relationship to natural diiron proteins, our analysis also showed that the DF1 bundle has more regular helices and the bundle tends to have smaller helix 1−1′ and 2−2′ distances, resulting in a compression of the active site. It will be interesting to determine the extent to which this compression restricts conformational changes required for the formation of critical catalytic intermediates.

Supporting Information Available: Coordination geometry of the "external" ions is depicted in Figure S1. This material is available free of charge via the Internet at http://pubs.acs.org.

JA054199X